

**SENSITIVITY OF EVAPOTRANSPIRATION AND
RUNOFF TO CLIMATE CHANGE IN THE MUDA
RIVER BASIN, MALAYSIA**

ZHANG DANDAN

UNIVERSITI SAINS MALAYSIA

2025

**SENSITIVITY OF EVAPOTRANSPIRATION AND
RUNOFF TO CLIMATE CHANGE IN THE MUDA
RIVER BASIN, MALAYSIA**

by

ZHANG DANDAN

**Thesis submitted in fulfilment of the requirements
for the degree of
Doctor of Philosophy**

June 2025

ACKNOWLEDGEMENT

Time flies, and as I reflect on my journey pursuing a Ph.D. in Malaysia, I am filled with mixed emotion. First and foremost, I would like to express my sincere gratitude to my main supervisor Associate Professor Gs. Dr. Tan Mou Leong, and co-supervisor, Associate Professor Dr. Sharifah Rohayah Binti Sheikh Dawood.

Throughout my studies, Dr. Tan provided continuous support and encouragement, inspiring me to persevere through the challenges of the learning process. He often emphasized that writing a thesis is an exploration, his continuous feedback and multiple revisions of my paper, along with his valuable suggestions, ultimately led to its publication in a Q2 journal.

I would like to extend my sincere appreciation to Dr. Sharifah for generously sharing her professional knowledge and expertise. Her kindness and support made a meaningful difference in both my studies and personal life. I am incredibly thankful to both of my supervisors for their invaluable guidance and encouragement.

Thanks to Miss Tew Yi Lin, I am truly appreciative of her kindness and support. I am deeply grateful to my parents and my son, who have been my source of motivation and support to continue to study. They are my pillar of strength. I would like to thank my husband, Wang Shuo, for his constant encouragement and assistance during difficult times.

Finally, special thanks to the Ministry of Higher Education for supporting this research through the Long-term Research Grant Scheme (grant no. LRGS/1/2020/UKM-USM/01/6/2), entitled “Impacts of weather and climate extremes under global warming of 1.5°C and 2.0°C on water balance in the Kelantan and Muda River Basins”.

TABLE OF CONTENTS

ACKNOWLEDGEMENT	ii
TABLE OF CONTENTS	iii
LIST OF TABLES	vi
LIST OF FIGURES	ix
LIST OF SYMBOLS	xxvii
LIST OF ABBREVIATIONS	xxviii
ABSTRAK	xxxii
ABSTRACT	xxxiii
CHAPTER 1 INTRODUCTION	1
1.1 Background of Study	1
1.2 Problem Statement	8
1.3 Research Questions	10
1.4 Research Objectives	10
1.5 Significance of the Study	11
1.6 Scope of the Study.....	12
1.7 Structure of Thesis	13
CHAPTER 2 LITERATURE REVIEW	15
2.1 Introduction	15
2.2 Hydrological Cycle	16
2.3 Climate Change Impact on Hydrology.....	20
2.4 Evapotranspiration, Runoff and Sensitivity Analysis	22
2.5 Climate Change Impacts on Water Resources	23
2.6 Hydrological Modelling	24

2.7	Climate Data.....	28
2.8	CMADS.....	29
2.9	Climate Data Performance Analysis	30
2.10	Climate Change and Hydrological Modelling	31
2.11	Climate Scenario	33
2.12	Climate Change Impacts on Runoff	35
2.13	Climate Change Impacts on Runoff in Malaysia	39
2.14	Conceptual Framework	40
2.15	Summary	44
	CHAPTER 3 METHODOLOGY.....	46
3.1	Introduction	46
3.2	Study Area.....	47
3.3	Data	49
3.4	SWAT Model	58
3.5	SWAT Set Up.....	64
3.6	Basin Delineation and River Network Formation.....	67
3.7	HRUs Separation.....	68
3.8	Sub-basin Characteristics	69
3.9	SWAT Calibration.....	70
3.10	SWAT Validation.....	73
3.11	Statistical Metrics	75
3.12	Climate Change Scenarios	76
3.13	Hydrological Index Selection.....	79
3.14	Summary	80

CHAPTER 4	RESULTS AND DISCUSSION	81
4.1	Introduction	81
4.2	Sensitivity Analysis, Calibration, and Validation	81
4.3	Comparison of CMADS and NCEP-CFSR.....	93
4.4	Individual Scenario	100
4.5	Water Balance Variations: Combined Scenarios	169
4.6	Discussion	254
4.7	Summary	263
CHAPTER 5	CONCLUSIONS AND RECOMMENDATIONS.....	266
5.1	Conclusions	266
5.2	Recommendations for Future Work.....	269
REFERENCES.....		271
LIST OF PUBLICATIONS		

LIST OF TABLES

	Page
Table 2.1	Description of satellite-based / reanalysis rainfall datasets used in the study.29
Table 3.1	Basic information of NCEP-CFSR and CMADS.51
Table 3.2	Observed monthly streamflow data from 2009 to 2013.....56
Table 3.3	Calculation methods of the parameters of the weather generator database65
Table 3.4	Parameters and definitions required for soil database construction...66
Table 3.5	The monthly water consumption data for the Muda Reservoir was obtained from the Department of Irrigation and Drainage Malaysia for the period 2009 to 2013.68
Table 3.6	The main geographic characteristics of 52 sub-basins of the MRB ..69
Table 3.7	Description of the streamflow parameters72
Table 3.8	General performance ratings for the monthly time step in hydrological simulation (Moriassi et al., 2007).....76
Table 3.9	Climate change scenarios design78
Table 4.1	Statistics of the evaluation indicators of the whole simulation period for the sensitivity analysis of streamflow simulation in SWAT forced by CMADS82
Table 4.2	Statistics of the Deviations of the NSE Value for the Changing Single Parameter During the One-at-a-Time Sensitivity Analysis for the SWAT Model Forced by the CMADS84
Table 4.3	The calibration results of the sensitive parameters for the SWAT model forced by CMADS85
Table 4.4	The evaluation indicators for the calibration and validation periods for the SWAT model forced by the CMADS.....86

Table 4.5	Statistics of the evaluation indicators of the whole simulation period for the sensitivity analysis of streamflow simulation in SWAT forced by NCEP-CFSR.....	88
Table 4.6	Statistics of the Deviations of the NSE value for the Changing Single Parameter During the One-at-a-Time Sensitivity Analysis for the SWAT Model Forced by the NCEP-CFSR	90
Table 4.7	The calibration results of the sensitive parameters for the SWAT model forced by the NCEP-CFSR	91
Table 4.8	The evaluation indicators for the calibration and validation periods for the SWAT model forced by the NCEP-CFSR.....	92
Table 4.9	The comparisons of the simulated average monthly and annual water yields of the SWAT model forced by the CMADS and NCEP-CFSR and measured water yields within the MRB.....	96
Table 4.10	The comparisons of the average monthly and annual precipitation during 2009-2013 of CMADS and NCEP-CFSR and measured water yields within the MRB	100
Table 4.11	Annual average value of the total runoff, surface runoff, underground runoff, and evapotranspiration for different SP and ST scenarios	102
Table 4.12	Seasonal average value of the total runoff, surface runoff, underground runoff, and evapotranspiration for different SP and ST scenarios	110
Table 4.13	Monthly average value of the total runoff for different SP and ST scenarios.....	128
Table 4.14	Monthly average value of the surface runoff for different SP and ST scenarios	131
Table 4.15	Monthly average value of the underground runoff for different SP and ST scenarios	134
Table 4.16	Monthly average value of the evapotranspiration for different SP and ST scenarios	137

Table 4.17	Annual average value of the total runoff, surface runoff, underground runoff, and evapotranspiration for S0- P+30%T+2°C scenarios	172
Table 4.18	Seasonal average value of the total runoff, surface runoff, underground runoff, and evapotranspiration for S0- P+30%T+2°C scenarios	179
Table 4.19	Monthly average value and change value (rate) of the total runoff for S0- P+30%T+2°C scenarios	201
Table 4.20	Monthly average value and change value (rate) of the surface runoff for S0- P+30%T+2°C scenarios	204
Table 4.21	Monthly average value and change value (rate) of the underground runoff for S0- P+30%T+2°C scenarios.....	207
Table 4.22	Monthly average value and change value (rate) of the evapotranspiration for S0- P+30%T+2°C scenarios	210

LIST OF FIGURES

	Page
Figure 2.1	Tropical hydrological cycle (Wohl et al., 2012). 19
Figure 2.2	Hydrological model classification (source: modified from Bourdin et al. (2012)).....25
Figure 2.3	Conceptual framework of this study.41
Figure 3.1	Hydro-climatic assessment methodology flow46
Figure 3.2	Muda River basin.49
Figure 3.3	Land use land cover of the MRB (Tan, Tew, et al., 2021).....51
Figure 3.4	Soil map of the MRB57
Figure 3.5	The schematic diagram of the hydrological processes in the SWAT model (Source: Neitsch et al. (2011)).....59
Figure 3.6	SWAT modelling procedure64
Figure 3.7	River network of the Muda River Basin.67
Figure 3.8	Elevation and slope distribution of the MRB.....70
Figure 4.1	Comparison of the measured streamflow and simulated streamflow when calibrating all 26 parameters for the SWAT model forced by CMADS83
Figure 4.2	Comparison of the calibration and validation results and the measured streamflow process for the SWAT model forced by the CMADS87
Figure 4.3	Comparison of the measured streamflow and simulated streamflow when calibrating all 26 parameters for the SWAT model forced by NCEP-CFSR89
Figure 4.4	Comparison of the calibration and validation results and the measured streamflow process for the SWAT model forced by the NCEP-CFSR93

Figure 4.5	Comparison of the annual water yields simulated by the SWAT model forced by the CMADS and NCEP-CFSR and the measured annual water yields within the MRB.....	94
Figure 4.6	Comparison of the monthly water yields simulated by the SWAT model forced by the CMADS and NCEP-CFSR and the measured monthly water yields within the MRB	95
Figure 4.7	Distributions of the CMADS and NCEP-CFSR virtual stations within the MRB.....	97
Figure 4.8	Comparison of the annual precipitation of CMADS and NCEP-CFSR and the measured annual water yields within the MRB	98
Figure 4.9	Comparison of the monthly precipitation of CMADS and NCEP-CFSR and the measured monthly water yields within the MRB	99
Figure 4.10	Statistic of the annual average total runoff, surface runoff, underground runoff, and evapotranspiration for the watersheds under S0, P-15%(SP1), P-30%(SP2), P+15%(SP3), P+30%(SP4) and T+1.5°C(ST1), T+2°C(ST2) scenarios.....	105
Figure 4.11	Spatial distribution of the annual average total runoff (TR), surface runoff (SR), underground runoff (UR) and evapotranspiration (E) within the MRB under different P-15%(SP1), P-30%(SP2), P+15%(SP3), P+30%(SP4) and T+1.5°C(ST1), T+2°C(ST2) scenarios.....	106
Figure 4.12	Spatial distribution of the change rate of the annual average total runoff (TR), surface runoff (SR), underground runoff (UR), and evapotranspiration (E) within the MRB under different P-15%(SP1), P-30%(SP2), P+15%(SP3), P+30%(SP4) and T+1.5°C(ST1), T+2°C(ST2) scenarios.....	107
Figure 4.13	Statistic of the seasonal average total runoff for the watersheds under S0, P-15%(SP1), P-30%(SP2), P+15%(SP3), P+30%(SP4) and T+1.5°C(ST1), T+2°C(ST2) scenarios.....	113

Figure 4.14	Spatial distribution of the seasonal average total runoff (TR) within the MRB under different P-15%(SP1), P-30%(SP2), P+15%(SP3), P+30%(SP4) and T+1.5 °C (ST1), T+2°C(ST2) scenarios.....	114
Figure 4.15	Spatial distribution of the change rate of the seasonal average total runoff within the MRB under different P-15%(SP1), P-30%(SP2), P+15%(SP3), P+30%(SP4) and T+1.5°C(ST1), T+2°C(ST2) scenarios.....	116
Figure 4.16	Statistic of the seasonal average surface runoff for the watersheds under S0, P-15%(SP1), P-30%(SP2), P+15%(SP3), P+30%(SP4) and T+1.5°C(ST1), T+2°C(ST2) scenarios.....	118
Figure 4.17	Spatial distribution of the seasonal average surface runoff (SR) within the MRB under different P-15%(SP1), P-30%(SP2), P+15%(SP3), P+30%(SP4) and T+1.5°C(ST1), T+2°C(ST2) scenarios.....	119
Figure 4.18	Spatial distribution of the change rate of the seasonal average surface runoff within the MRB under different P-15%(SP1), P-30%(SP2), P+15%(SP3), P+30%(SP4) and T+1.5°C(ST1), T+2°C(ST2) scenarios.....	120
Figure 4.19	Statistic of the seasonal average underground runoff for the watersheds under S0, P-15%(SP1), P-30%(SP2), P+15%(SP3), P+30%(SP4) and T+1.5°C(ST1), T+2°C(ST2) scenarios.....	121
Figure 4.20	Spatial distribution of the seasonal average underground runoff (UR) within the MRB under different P-15%(SP1), P-30%(SP2), P+15%(SP3), P+30%(SP4) and T+1.5°C(ST1), T+2°C(ST2) scenarios.....	122
Figure 4.21	Spatial distribution of the change rate of the seasonal average underground runoff within the MRB under different P-15%(SP1), P-30%(SP2), P+15%(SP3), P+30%(SP4) and T+1.5°C(ST1), T+2°C(ST2) scenarios.....	123

Figure 4.22	Statistic of the seasonal average evapotranspiration for the watersheds under S0, P-15%(SP1), P-30%(SP2), P+15%(SP3), P+30%(SP4), T+1.5°C(ST1), T+2°C(ST2) scenarios.	124
Figure 4.23	Spatial distribution of the seasonal average evapotranspiration (E) within the MRB under different P-15%(SP1), P-30%(SP2), P+15%(SP3), P+30%(SP4)and T+1.5°C(ST1), T+2°C(ST2) scenarios.....	125
Figure 4.24	Spatial distribution of the change rate of the seasonal average evapotranspiration within the MRB under different P-15%(SP1), P-30%(SP2), P+15%(SP3), P+30%(SP4) and T+1.5°C(ST1), T+2°C(ST2) scenarios.....	127
Figure 4.25	Statistic of the monthly average total runoff for the watersheds under S0, P-15%(SP1), P-30%(SP2), P+15%(SP3), P+30%(SP4) and T+1.5°C(ST1), T+2°C(ST2) scenarios for January, February, March, and April.	139
Figure 4.26	Statistic of the monthly average total runoff for the watersheds under S0, P-15%(SP1), P-30%(SP2), P+15%(SP3), P+30%(SP4) and T+1.5°C(ST1), T+2°C(ST2) scenarios for May, June, July, and August.	140
Figure 4.27	Statistic of the monthly average total runoff for the watersheds under S0, P-15%(SP1), P-30%(SP2), P+15%(SP3), P+30%(SP4) and T+1.5°C(ST1), T+2°C(ST2) scenarios for September, October, November, and December.....	140
Figure 4.28	Spatial distribution of the monthly average total runoff (TR) within the MRB under different P-15%(SP1), P-30%(SP2), P+15%(SP3), P+30%(SP4) and T+1.5°C(ST1), T+2°C(ST2) scenarios for January to June.	142
Figure 4.29	Spatial distribution of the monthly average total runoff (TR) within the MRB under different P-15%(SP1), P-30%(SP2),	

	P+15%(SP3), P+30%(SP4) and T+1.5°C(ST1), T+2°C(ST2) scenarios for July to December.	143
Figure 4.30	Spatial distribution of the change rate of the monthly average total runoff within the MRB under different P-15%(SP1), P-30%(SP2), P+15%(SP3), P+30%(SP4) and T+1.5°C(ST1), T+2°C(ST2) scenarios for January to June.	144
Figure 4.31	Spatial distribution of the change rate of the monthly average total runoff within the MRB under different P-15%(SP1), P-30%(SP2), P+15%(SP3), P+30%(SP4) and T+1.5°C(ST1), T+2°C(ST2) scenarios for July to December.	146
Figure 4.32	Statistic of the monthly average surface runoff for the watersheds under S0, P-15%(SP1), P-30%(SP2), P+15%(SP3), P+30%(SP4) and T+1.5°C(ST1), T+2°C(ST2) scenarios for January, February, March, and April.	147
Figure 4.33	Statistic of the monthly average surface runoff for the watersheds under S0, P-15%(SP1), P-30%(SP2), P+15%(SP3), P+30%(SP4) and T+1.5°C(ST1), T+2°C(ST2) scenarios for May, June, July, and August.	148
Figure 4.34	Statistic of the monthly average surface runoff for the watersheds under S0, P-15%(SP1), P-30%(SP2), P+15%(SP3), P+30%(SP4) and T+1.5°C(ST1), T+2°C(ST2) scenarios for September, October, November, and December.	149
Figure 4.35	Spatial distribution of the monthly average surface runoff (SR) within the MRB under different P-15%(SP1), P-30%(SP2), P+15%(SP3), P+30%(SP4) and T+1.5°C(ST1), T+2°C(ST2) scenarios for January to June.	150
Figure 4.36	Spatial distribution of the monthly average surface runoff (SR) within the MRB under different P-15%(SP1), P-30%(SP2), P+15%(SP3), P+30%(SP4) and T+1.5°C(ST1), T+2°C(ST2) scenarios for July to December.	151

Figure 4.37	Spatial distribution of the change rate of the monthly average surface runoff within the MRB under different P-15%(SP1), P-30%(SP2), P+15%(SP3), P+30%(SP4) and T+1.5°C(ST1), T+2°C(ST2) scenarios for January to June.	152
Figure 4.38	Spatial distribution of the change rate of the monthly average surface runoff within the MRB under different P-15%(SP1), P-30%(SP2), P+15%(SP3), P+30%(SP4) and T+1.5°C(ST1), T+2°C(ST2) scenarios for July to December.	153
Figure 4.39	Statistic of the monthly average underground runoff for the watersheds under S0, P-15%(SP1), P-30%(SP2), P+15%(SP3), P+30%(SP4), and T+1.5°C(ST1), T+2°C(ST2) scenarios for January, February, March, and April.	154
Figure 4.40	Statistic of the monthly average underground runoff for the watersheds under S0, P-15%(SP1), P-30%(SP2), P+15%(SP3), P+30%(SP4) , and T+1.5°C(ST1), T+2°C(ST2) scenarios for May, June, July, and August.	154
Figure 4.41	Statistic of the monthly average underground runoff for the watersheds under S0, P-15%(SP1), P-30%(SP2), P+15%(SP3), P+30%(SP4), and T+1.5°C(ST1), T+2°C(ST2) scenarios for September, October, November, and December.....	155
Figure 4.42	Spatial distribution of the monthly average underground runoff (UR) within the MRB under different P-15%(SP1), P-30%(SP2), P+15%(SP3), P+30%(SP4), and T+1.5°C(ST1), T+2°C(ST2) scenarios for January to June.	156
Figure 4.43	Spatial distribution of the monthly average underground runoff (UR) within the MRB under different P-15%(SP1), P-30%(SP2), P+15%(SP3), P+30%(SP4) , and T+1.5°C(ST1), T+2°C(ST2) scenarios for July to December.	158
Figure 4.44	Spatial distribution of the change rate of the monthly average underground runoff within the MRB under different P-15%(SP1),	

	P-30%(SP2), P+15%(SP3), P+30%(SP4), and T+1.5°C(ST1), T+2°C(ST2) scenarios for January to June.	159
Figure 4.45	Spatial distribution of the change rate of the monthly average underground runoff within the MRB under different P-15%(SP1), P-30%(SP2), P+15%(SP3), P+30%(SP4), and T+1.5°C(ST1), T+2°C(ST2) scenarios for July to December.	160
Figure 4.46	Statistic of the monthly average evapotranspiration for the watersheds under S0, P-15%(SP1), P-30%(SP2), P+15%(SP3), P+30%(SP4) and T+1.5°C(ST1), T+2°C(ST2) scenarios for January, February, March, and April.	163
Figure 4.47	Statistic of the monthly average evapotranspiration for the watersheds under S0, P-15%(SP1), P-30%(SP2), P+15%(SP3), P+30%(SP4) and T+1.5°C(ST1), T+2°C(ST2) scenarios for May, June, July, and August.	163
Figure 4.48	Statistic of the monthly average evapotranspiration for the watersheds under S0, P-15%(SP1), P-30%(SP2), P+15%(SP3), P+30%(SP4) and T+1.5°C(ST1), T+2°C(ST2) scenarios for September, October, November, and December.	164
Figure 4.49	Spatial distribution of the monthly average evapotranspiration (E) within the MRB under different P-15%(SP1), P-30%(SP2), P+15%(SP3), P+30%(SP4) and T+1.5°C(ST1), T+2°C(ST2) scenarios for January to June.	165
Figure 4.50	Spatial distribution of the monthly average evapotranspiration(E) within the MRB under different P-15%(SP1), P-30%(SP2), P+15%(SP3), P+30%(SP4) and T+1.5°C(ST1), T+2°C(ST2) scenarios for July to December.	166
Figure 4.51	Spatial distribution of the change rate of the monthly average evapotranspiration within the MRB under different P-15%(SP1),	

	P-30%(SP2), P+15%(SP3), P+30%(SP4) and T+1.5°C(ST1), T+2°C(ST2) scenarios for January to June.	167
Figure 4.52	Spatial distribution of the change rate of the monthly average evapotranspiration within the MRB under different P-15%(SP1), P-30%(SP2), P+15%(SP3), P+30%(SP4) and T+1.5°C(ST1), T+2°C(ST2) scenarios for July to December.	168
Figure 4.53	Statistic of the annual average total runoff (TR), surface runoff (SR), underground runoff (UR), and evapotranspiration (E) for the watersheds under S0, P-15%T+1.5°C(S1), P-15%T+2°C(S2), P-30%T+1.5°C(S3), P-30%T+2°C(S4), P+15%T+1.5°C(S5), P+15%T+2°C(S6), P+30%T+1.5°C(S7), P+30%T+2°C(S8) scenarios	173
Figure 4.54	Spatial distribution of the annual average total runoff (TR), surface runoff (SR), underground runoff (UR) , and evapotranspiration (E) within the MRB under S0, P-15%T+1.5° C(S1), P-15%T+2°C(S2), P-30%T+1.5°C(S3), P-30%T+2°C(S4) scenarios.	174
Figure 4.55	Spatial distribution of the annual average total runoff (TR) , surface runoff (SR) , underground runoff (UR), and evapotranspiration (E) within the MRB under S0 and P+15%T+1.5°C(S5), P+15%T+2°C(S6), P+30%T+1.5°C(S7), P+30%T+2°C(S8) scenarios.	175
Figure 4.56	Spatial distribution of the change rate of the annual average total runoff (TR), surface runoff (SR), underground runoff (UR), and evapotranspiration (E)within the MRB under S0, P- 15%T+1.5(S1), P-15%T+2°C(S2), P-30%T+1.5°C(S3), P- 30%T+2°C(S4) scenarios.....	176
Figure 4.57	Spatial distribution of the change rate of the annual average total runoff (TR), surface runoff (SR), underground runoff (UR), and	

	evapotranspiration (E) within the MRB under S0 and P+15%T+1.5°C(S5), P+15%T+2°C(S6), P+30%T+1.5°C(S7), P+30%T+2°C(S8) scenarios.	177
Figure 4.58	Statistic of the seasonal average total runoff for the watersheds under S0, P-15%T+1.5°C(S1), P-15%T+2°C(S2), P-30%T+1.5°C(S3), P-30%T+2°C(S4), P+15%T+1.5°C(S5), P+15%T+2°C(S6), P+30%T+1.5°C(S7), P+30%T+2°C(S8) scenarios.	182
Figure 4.59	Spatial distribution of the seasonal average total runoff (TR) within the MRB under S0 P-15%T+1.5°C(S1), P-15%T+2°C(S2), P-30%T+1.5°C(S3), P-30%T+2°C(S4) scenarios.	183
Figure 4.60	Spatial distribution of the seasonal average total runoff (TR) within the MRB under S0 and P+15%T+1.5°C(S5), P+15%T+2°C(S6), P+30%T+1.5°C(S7), P+30%T+2°C(S8) scenarios.	184
Figure 4.61	Spatial distribution of the change rate of the annual average total runoff within the MRB under S0, P-15%T+1.5°C(S1), P-15%T+2°C(S2), P-30%T+1.5°C(S3), P-30%T+2°C(S4) scenarios.	186
Figure 4.62	Spatial distribution of the change rate of the annual average total runoff within the MRB under S0 and P+15%T+1.5°C(S5), P+15%T+2°C(S6), P+30%T+1.5°C(S7), P+30%T+2°C(S8) scenarios.	186
Figure 4.63	Statistic of the seasonal average surface runoff for the watersheds under S0, P-15%T+1.5°C(S1), P-15%T+2°C(S2), P-30%T+1.5°C(S3), P-30%T+2°C(S4), P+15%T+1.5°C(S5), P+15%T+2°C(S6), P+30%T+1.5°C(S7), P+30%T+2°C(S8) scenarios.	187
Figure 4.64	Spatial distribution of the seasonal average surface runoff (SR) within the MRB under S0, P-15%T+1.5°C(S1), P-15%T+2°C(S2), P-30%T+1.5°C(S3), P-30%T+2°C(S4) scenarios.	188

Figure 4.65	Spatial distribution of the seasonal average surface runoff (SR) within the MRB under S0 and P+15%T+1.5°C(S5), P+15%T+2°C(S6), P+30%T+1.5°C(S7), P+30%T+2°C(S8) scenarios.	189
Figure 4.66	Spatial distribution of the change rate of the annual average surface runoff within the MRB under S0, P-15%T+1.5°C(S1), P-15%T+2°C(S2), P-30%T+1.5°C(S3), P-30%T+2°C(S4) scenarios.	190
Figure 4.67	Spatial distribution of the change rate of the annual average surface runoff within the MRB under S0 and P+15%T+1.5°C(S5), P+15%T+2°C(S6), P+30%T+1.5°C(S7), P+30%T+2°C(S8) scenarios.	190
Figure 4.68	Statistic of the seasonal average underground runoff for the watersheds under S0, P-15%T+1.5°C(S1), P-15%T+2°C(S2), P-30%T+1.5°C(S3), P-30%T+2°C(S4), P+15%T+1.5°C(S5), P+15%T+2°C(S6), P+30%T+1.5°C(S7), P+30%T+2°C(S8) scenarios.	191
Figure 4.69	Spatial distribution of the seasonal average underground runoff (UR) within the MRB under S0, P-15%T+1.5°C(S1), P-15%T+2°C(S2), P-30%T+1.5°C(S3), P-30%T+2°C(S4) scenarios.	192
Figure 4.70	Spatial distribution of the seasonal average underground runoff (UR) within the MRB under S0 and P+15%T+1.5°C(S5), P+15%T+2°C(S6), P+30%T+1.5°C(S7), P+30%T+2°C(S8) scenarios.	193
Figure 4.71	Spatial distribution of the change rate of the annual average underground runoff within the MRB under S0, P-15%T+1.5°C(S1), P-15%T+2°C(S2), P-30%T+1.5°C(S3), P-30%T+2°C(S4) scenarios.	194
Figure 4.72	Spatial distribution of the change rate of the annual average underground runoff within the MRB under S0 and P+15%T+1.5°C	

	C(S5), P+15%T+2°C(S6), P+30%T+1.5°C(S7), P+30%T+2°C(S8) scenarios.	195
Figure 4.73	Statistic of the seasonal average evapotranspiration for the watersheds under S0, P-15%T+1.5°C(S1), P-15%T+2°C(S2), P-30%T+1.5°C(S3), P-30%T+2°C(S4), P+15%T+1.5°C(S5), P+15%T+2°C(S6), P+30%T+1.5°C(S7), P+30%T+2°C(S8) scenarios.	196
Figure 4.74	Spatial distribution of the seasonal average evapotranspiration (E) within the MRB under S0, P-15%T+1.5°C(S1), P-15%T+2°C(S2), P-30%T+1.5°C(S3), P-30%T+2°C(S4) scenarios.	197
Figure 4.75	Spatial distribution of the seasonal average evapotranspiration (E) within the MRB under S0 and P+15%T+1.5°C(S5), P+15%T+2°C(S6), P+30%T+1.5°C(S7), P+30%T+2°C(S8) scenarios.	198
Figure 4.76	Spatial distribution of the change rate of the annual average evapotranspiration within the MRB under P-15%T+1.5°C(S1), P-15%T+2°C(S2), P-30%T+1.5°C(S3), P-30%T+2°C(S4) scenarios.	199
Figure 4.77	Spatial distribution of the change rate of the annual average evapotranspiration within the MRB under S0 and P+15%T+1.5°C(S5)- P+30%(S8)scenarios.	199
Figure 4.78	Statistic of the monthly average total runoff for the watersheds under S0, P-15%T+1.5°C(S1), P-15%T+2°C(S2), P-30%T+1.5°C(S3), P-30%T+2°C(S4), P+15%T+1.5°C(S5), P+15%T+2°C(S6), P+30%T+1.5°C(S7), P+30%T+2°C(S8) scenarios for January, February, March, and April.	213
Figure 4.79	Statistic of the monthly average total runoff for the watersheds under S0, P-15%T+1.5°C(S1), P-15%T+2°C(S2), P-30%T+1.5°C(S3), P-30%T+2°C(S4), P+15%T+1.5°C(S5), P+15%T+2°C(S6), P+30%T+1.5°C(S7), P+30%T+2°C(S8) scenarios for May, June, July, and August.	213

	C(S6), P+30%T+1.5°C(S7), P+30%T+2°C(S8) scenarios for May, June, July, and August.	213
Figure 4.80	Statistic of the monthly average total runoff for the watersheds under S0, P-15%T+1.5°C(S1), P-15%T+2°C(S2), P-30%T+1.5° C(S3), P-30%T+2°C(S4), P+15%T+1.5°C(S5), P+15%T+2° C(S6), P+30%T+1.5°C(S7), P+30%T+2°C(S8) scenarios for September, October, November, and December.....	214
Figure 4.81	Spatial distribution of the monthly average total runoff (TR) within the MRB under S0, P-15%T+1.5°C(S1), P-15%T+2° C(S2), P-30%T+1.5°C(S3), P-30%T+2°C(S4), P+15%T+1.5° C(S5), P+15%T+2°C(S6), P+30%T+1.5°C(S7), P+30%T+2° C(S8) scenarios for January to April.....	217
Figure 4.82	Spatial distribution of the monthly average total runoff (TR) within the MRB under S0, P-15%T+1.5°C(S1), P-15%T+2° C(S2), P-30%T+1.5°C(S3), P-30%T+2°C(S4), P+15%T+1.5° C(S5), P+15%T+2°C(S6), P+30%T+1.5°C(S7), P+30%T+2° C(S8) scenarios for May to August.....	218
Figure 4.83	Spatial distribution of the monthly average total runoff (TR) within the MRB under S0, P-15%T+1.5°C(S1), P-15%T+2° C(S2), P-30%T+1.5°C(S3), P-30%T+2°C(S4), P+15%T+1.5° C(S5), P+15%T+2°C(S6), P+30%T+1.5°C(S7), P+30%T+2° C(S8) scenarios for September to December.	219
Figure 4.84	Spatial distribution of the change rate of the monthly average total runoff within the MRB under S0, P-15%T+1.5°C(S1), P- 15%T+2°C(S2), P-30%T+1.5°C(S3), P-30%T+2°C(S4), P+15%T+1.5°C(S5), P+15%T+2°C(S6), P+30%T+1.5°C(S7), P+30%T+2°C(S8) scenarios for January to April.....	220

Figure 4.85	Spatial distribution of the change rate of the monthly average total runoff within the MRB under S0, P-15%T+1.5°C(S1), P-15%T+2°C(S2), P-30%T+1.5°C(S3), P-30%T+2°C(S4), P+15%T+1.5°C(S5), P+15%T+2°C(S6), P+30%T+1.5°C(S7), P+30%T+2°C(S8) scenarios for May to August.....	221
Figure 4.86	Spatial distribution of the change rate of the monthly average total runoff within the MRB under S0, P-15%T+1.5°C(S1), P-15%T+2°C(S2), P-30%T+1.5°C(S3), P-30%T+2°C(S4), P+15%T+1.5°C(S5), P+15%T+2°C(S6), P+30%T+1.5°C(S7), P+30%T+2°C(S8) scenarios for September to December.	222
Figure 4.87	Statistic of the monthly average surface runoff for the watersheds under S0, P-15%T+1.5°C(S1), P-15%T+2°C(S2), P-30%T+1.5°C(S3), P-30%T+2°C(S4), P+15%T+1.5°C(S5), P+15%T+2°C(S6), P+30%T+1.5°C(S7), P+30%T+2°C(S8) scenarios for January, February, March, and April.	224
Figure 4.88	Statistic of the monthly average surface runoff for the watersheds under S0, P-15%T+1.5°C(S1), P-15%T+2°C(S2), P-30%T+1.5°C(S3), P-30%T+2°C(S4), P+15%T+1.5°C(S5), P+15%T+2°C(S6), P+30%T+1.5°C(S7), P+30%T+2°C(S8) scenarios for May, June, July, and August.	224
Figure 4.89	Statistic of the monthly average surface runoff for the watersheds under S0, P-15%T+1.5°C(S1), P-15%T+2°C(S2), P-30%T+1.5°C(S3), P-30%T+2°C(S4), P+15%T+1.5°C(S5), P+15%T+2°C(S6), P+30%T+1.5°C(S7), P+30%T+2°C(S8) scenarios for September, October, November, and December.....	225
Figure 4.90	Spatial distribution of the monthly average surface runoff (SR) within the MRB under S0, P-15%T+1.5°C(S1), P-15%T+2°C(S2), P-30%T+1.5°C(S3), P-30%T+2°C(S4), P+15%T+1.5°C(S5), P+15%T+2°C(S6), P+30%T+1.5°C(S7), P+30%T+2°C(S8) scenarios for September, October, November, and December.....	225

	C(S5), P+15%T+2°C(S6), P+30%T+1.5°C(S7), P+30%T+2°C(S8) scenarios for January to April.....	227
Figure 4.91	Spatial distribution of the monthly average surface runoff (SR) within the MRB under S0, P-15%T+1.5°C(S1), P-15%T+2°C(S2), P-30%T+1.5°C(S3), P-30%T+2°C(S4), P+15%T+1.5°C(S5), P+15%T+2°C(S6), P+30%T+1.5°C(S7), P+30%T+2°C(S8) scenarios for May to August.....	228
Figure 4.92	Spatial distribution of the monthly average surface (SR) runoff within the MRB under S0, P-15%T+1.5°C(S1), P-15%T+2°C(S2), P-30%T+1.5°C(S3), P-30%T+2°C(S4), P+15%T+1.5°C(S5), P+15%T+2°C(S6), P+30%T+1.5°C(S7), P+30%T+2°C(S8) scenarios for September to December.	229
Figure 4.93	Spatial distribution of the change rate of the monthly average surface runoff within the MRB under S0, P-15%T+1.5°C(S1), P-15%T+2°C(S2), P-30%T+1.5°C(S3), P-30%T+2°C(S4), P+15%T+1.5°C(S5), P+15%T+2°C(S6), P+30%T+1.5°C(S7), P+30%T+2°C(S8) scenarios for January to April.....	230
Figure 4.94	Spatial distribution of the change rate of the monthly average surface runoff within the MRB under S0, P-15%T+1.5°C(S1), P-15%T+2°C(S2), P-30%T+1.5°C(S3), P-30%T+2°C(S4), P+15%T+1.5°C(S5), P+15%T+2°C(S6), P+30%T+1.5°C(S7), P+30%T+2°C(S8) scenarios for May to August.....	231
Figure 4.95	Spatial distribution of the change rate of the monthly average surface runoff within the MRB under S0, P-15%T+1.5°C(S1), P-15%T+2°C(S2), P-30%T+1.5°C(S3), P-30%T+2°C(S4), P+15%T+1.5°C(S5), P+15%T+2°C(S6), P+30%T+1.5°C(S7), P+30%T+2°C(S8) scenarios for September to December.	232

Figure 4.96	Statistic of the monthly average underground runoff for the watersheds under S0, P-15%T+1.5°C(S1), P-15%T+2°C(S2), P-30%T+1.5°C(S3), P-30%T+2°C(S4), P+15%T+1.5°C(S5), P+15%T+2°C(S6), P+30%T+1.5°C(S7), P+30%T+2°C(S8) scenarios for January, February, March, and April.....	234
Figure 4.97	Statistic of the monthly average underground runoff for the watersheds under S0, P-15%T+1.5°C(S1), P-15%T+2°C(S2), P-30%T+1.5°C(S3), P-30%T+2°C(S4), P+15%T+1.5°C(S5), P+15%T+2°C(S6), P+30%T+1.5°C(S7), P+30%T+2°C(S8) scenarios for May, June, July, and August.....	234
Figure 4.98	Statistic of the monthly average underground runoff for the watersheds under S0, P-15%T+1.5°C(S1), P-15%T+2°C(S2), P-30%T+1.5°C(S3), P-30%T+2°C(S4), P+15%T+1.5°C(S5), P+15%T+2°C(S6), P+30%T+1.5°C(S7), P+30%T+2°C(S8) scenarios for September, October, November, and December.	235
Figure 4.99	Spatial distribution of the monthly average underground runoff (UR) within the MRB under S0, P-15%T+1.5°C(S1), P-15%T+2°C(S2), P-30%T+1.5°C(S3), P-30%T+2°C(S4), P+15%T+1.5°C(S5), P+15%T+2°C(S6), P+30%T+1.5°C(S7), P+30%T+2°C(S8) scenarios for January to April.....	237
Figure 4.100	Spatial distribution of the monthly average underground runoff (UR) within the MRB under S0, P-15%T+1.5°C(S1), P-15%T+2°C(S2), P-30%T+1.5°C(S3), P-30%T+2°C(S4), P+15%T+1.5°C(S5), P+15%T+2°C(S6), P+30%T+1.5°C(S7), P+30%T+2°C(S8) scenarios for May to August.....	238
Figure 4.101	Spatial distribution of the monthly average underground runoff (UR) within the MRB under S0, P-15%T+1.5°C(S1), P-15%T+2°C(S2), P-30%T+1.5°C(S3), P-30%T+2°C(S4), P+15%T+1.5°C(S5), P+15%T+2°C(S6), P+30%T+1.5°C(S7), P+30%T+2°C(S8) scenarios for September to December.....	239

	C(S5), P+15% T+2°C(S6), P+30% T+1.5°C(S7), P+30% T+2°C(S8) scenarios for September to December.	239
Figure 4.102	Spatial distribution of the change rate of the monthly average underground runoff within the MRB under S0, P-15% T+1.5°C(S1), P-15% T+2°C(S2), P-30% T+1.5°C(S3), P-30% T+2°C(S4), P+15% T+1.5°C(S5), P+15% T+2°C(S6), P+30% T+1.5°C(S7), P+30% T+2°C(S8) scenarios for January to April.....	240
Figure 4.103	Spatial distribution of the change rate of the monthly average underground runoff within the MRB under S0, P-15% T+1.5°C(S1), P-15% T+2°C(S2), P-30% T+1.5°C(S3), P-30% T+2°C(S4), P+15% T+1.5°C(S5), P+15% T+2°C(S6), P+30% T+1.5°C(S7), P+30% T+2°C(S8) scenarios for May to August.....	241
Figure 4.104	Spatial distribution of the change rate of the monthly average underground runoff within the MRB under S0, P-15% T+1.5°C(S1), P-15% T+2°C(S2), P-30% T+1.5°C(S3), P-30% T+2°C(S4), P+15% T+1.5°C(S5), P+15% T+2°C(S6), P+30% T+1.5°C(S7), P+30% T+2°C(S8) scenarios for September to December.	242
Figure 4.105	Statistic of the monthly average evapotranspiration for the watersheds under S0, P-15% T+1.5°C(S1), P-15% T+2°C(S2), P-30% T+1.5°C(S3), P-30% T+2°C(S4), P+15% T+1.5°C(S5), P+15% T+2°C(S6), P+30% T+1.5°C(S7), P+30% T+2°C(S8) scenarios for January, February, March, and April.....	244
Figure 4.106	Statistic of the monthly average evapotranspiration for the watersheds under S0, P-15% T+1.5°C(S1), P-15% T+2°C(S2), P-30% T+1.5°C(S3), P-30% T+2°C(S4), P+15% T+1.5°C(S5), P+15% T+2°C(S6), P+30% T+1.5°C(S7), P+30% T+2°C(S8) scenarios for May, June, July, and August.....	244

- Figure 4.107 Statistic of the monthly average evapotranspiration for the watersheds under S0, P-15%T+1.5°C(S1), P-15%T+2°C(S2), P-30%T+1.5°C(S3), P-30%T+2°C(S4), P+15%T+1.5°C(S5), P+15%T+2°C(S6), P+30%T+1.5°C(S7), P+30%T+2°C(S8) scenarios for September, October, November, and December.245
- Figure 4.108 Spatial distribution of the monthly average evapotranspiration (E) within the MRB under S0, P-15%T+1.5°C(S1), P-15%T+2°C(S2), P-30%T+1.5°C(S3), P-30%T+2°C(S4), P+15%T+1.5°C(S5), P+15%T+2°C(S6), P+30%T+1.5°C(S7), P+30%T+2°C(S8) scenarios for January to April.....248
- Figure 4.109 Spatial distribution of the monthly average evapotranspiration (E) within the MRB under S0, P-15%T+1.5°C(S1), P-15%T+2°C(S2), P-30%T+1.5°C(S3), P-30%T+2°C(S4), P+15%T+1.5°C(S5), P+15%T+2°C(S6), P+30%T+1.5°C(S7), P+30%T+2°C(S8) scenarios for May to August.....249
- Figure 4.110 Spatial distribution of the monthly average evapotranspiration(E) within the MRB under S0, P-15%T+1.5°C(S1), P-15%T+2°C(S2), P-30%T+1.5°C(S3), P-30%T+2°C(S4), P+15%T+1.5°C(S5), P+15%T+2°C(S6), P+30%T+1.5°C(S7), P+30%T+2°C(S8) scenarios for September to December.250
- Figure 4.111 Spatial distribution of the change rate of the monthly average evapotranspiration (E) within the MRB under S0, P-15%T+1.5°C(S1), P-15%T+2°C(S2), P-30%T+1.5°C(S3), P-30%T+2°C(S4), P+15%T+1.5°C(S5), P+15%T+2°C(S6), P+30%T+1.5°C(S7), P+30%T+2°C(S8) scenarios for January to April.....251
- Figure 4.112 Spatial distribution of the change rate of the monthly average evapotranspiration within the MRB under S0, P-15%T+1.5°C(S1), P-15%T+2°C(S2), P-30%T+1.5°C(S3), P-30%T+2°C(S4),

P+15%T+1.5°C(S5), P+15%T+2°C(S6), P+30%T+1.5°C(S7),
P+30%T+2°C(S8) scenarios for May to August.....252

Figure 4.113 Spatial distribution of the change rate of the monthly average
surface runoff within the MRB under S0, P-15%T+1.5°C(S1), P-
15%T+2°C(S2), P-30%T+1.5°C(S3), P-30%T+2°C(S4),
P+15%T+1.5°C(S5), P+15%T+2°C(S6), P+30%T+1.5°C(S7),
P+30%T+2°C(S8) scenarios for September to December.253

LIST OF SYMBOLS

km	Kilometre
km ²	Square kilometre
mm/month	Milimetre per month
NSE	Nash sucliffe efficiency
R ²	Coefficient of determination
RSR	Ratio of root mean square error

LIST OF ABBREVIATIONS

Parameter	Detail
CHIRPS	Climate Hazards Group InfraRed Precipitation with Station data
CLAY1	Clay content of the first layer of soil
CMADS	China meteorological assimilation driving datasets
CMIP5	Coupled Model Intercomparison Project Phase 5
CMIP6	Coupled Model Intercomparison Project Phase 6
CREAMS	Chemicals Runoff and Erosion from Agricultural Management Systems
EPCI	Executive-Process/Interactive Control
ESA	European Space Agency
FAO	Food and Agricultural Organization
GCM	General Circulation Model
HRUs	Hydrological Response Units
HWSD	Harmonized World Soil Database
IPCC	Intergovernmental Panel on Climate Change
ISSCAS	Institute of Soil Research of the Chinese Academy of Sciences
JRC	Joint Research Centre of the European Commission
LULC	Land Use and Land Cover
ME	Median
MRB	MUDA River Basin
NCEP-CFSR	National Centers-Environmental Prediction-Climate Prediction System Reanalysis
NIMA	National Mapping Agency
NLAYERS	Number of layers in the soil
NOAA	National Oceanic and Atmospheric Administration
NSE	Nash efficiency coefficient
PB	Percentage bias
PERSIANN-CDR	Precipitation Estimation from Remotely Sensed Information Using Artificial Neural Network-Climate Data Record
POD	Proper orthogonal decomposition

RCP	Representative Concentration Pathway
RMSE	Root mean squared error
ROCK1	Rock fragment content of the first layer of soil
S	Scenarios
SAND1	Sand content of the first layer of soil
SCS	Soil Conservation Services
SDSM	Statistical Downscaling Model
SHE models	System Hydrological European
SILT1	Silt content of the first layer of soil
SOL_ALB1	Moist soil albedo of the first layer of soil
SOL_AWC1	Available water capacity of the first layer of soil
SOL_BD1	Moist bulk density of the first layer of soil
SOL_CAL1	Calcium carbonate content of the first layer of soil
SOL_CBN1	Organic carbon content of the first layer of soil
SOL_CRK	Crack volume potential of soil
SOL_EC1	Soil electrical conductivity of the first layer of soil
SOL_K1	Saturated hydraulic conductivity of the first layer of soil
SOL_PH1	Soil PH of the first layer of soil
SOL_Z1	Depth from soil surface to bottom of the first layer of soil
SOL_ZMX	Maximum rooting depth of soil profile
SP	Precipitation Scenarios
SPI	Standardised Precipitation Index
SRTM	National Aeronautics And Space Administration Shuttle Radar Topography Mission
SSI	Standardised current discharge index
ST	Temperature scenarios
SUFI-2	Sequential Uncertainty Fitting-2
SWAT	Soil and Water Assessment Tool
SWAT-CUP	SWAT Calibration And Uncertainty Procedures
SWMM	Storm water management models
SWRRB	Simulator for water resources in rural basins
TEXTURE	Texture of soil layer
TRMM3B42 V7	Tropical Rainfall Measuring Mission
UNEP	United Nations Environment Programme
USDA	Center of the United States Department of Agriculture

USLE_K1	USLE equation soil erodibility (K) factor of the first layer of soil
WMO	World Meteorological Organization
WY	Water Yields

KESENSITIFAN EVAPOTRANSPIRASI DAN AIR LARIAN TERHADAP PERUBAHAN IKLIM DI LEMBANGAN SUNGAI MUDA, MALAYSIA

ABSTRAK

Memahami bagaimana perubahan iklim mempengaruhi keseimbangan air di kawasan tropika adalah penting untuk membangunkan strategi inovatif dalam penyesuaian dan mitigasi perubahan iklim. Penilaian hidro-iklim sangat bergantung pada data iklim yang tepat; namun, penyelidikan iklim menghadapi cabaran dalam memperoleh data iklim cerapan bagi jangka panjang. Kajian ini bertujuan untuk menilai kesan perubahan iklim terhadap keseimbangan air di Lembangan Sungai Muda (MRB) dengan menggunakan data sumber terbuka. Pertama, kajian ini menilai kebolehpercayaan *China Meteorological Assimilation Driving Dataset for the Soil and Water Assessment Tool* (CMADS) dan *National Centres for Environmental Prediction Climate Forecast System Reanalysis* (NCEP-CFSR) dalam mensimulasikan perubahan iklim dan hidrologi di MRB. Data yang paling optimum kemudian digunakan untuk menjalankan model *Soil and Water Assessment Tool* (SWAT) bagi mengkaji kesan perubahan iklim terhadap keseimbangan air di bawah empat belas senario iklim sintetik, yang merangkumi peningkatan suhu sebanyak 1.5 °C dan 2 °C serta perubahan kerpasan antara -30% hingga +30%, berdasarkan kajian terdahulu. Hasil kajian menunjukkan bahawa peningkatan dalam kerpasan dan suhu menyebabkan peningkatan larian air permukaan. Model SWAT berjaya mensimulasikan larian air bulanan di MRB, dengan nilai NSE dan R² masing-masing sebanyak 0.57 dan 0.59. CMADS menunjukkan ketepatan yang lebih tinggi berbanding NCEP-CFSR, dengan nilai PBIAS dan RSR masing-masing 9.2% dan 0.66.

Walau bagaimanapun, prestasi model SWAT yang menggunakan data kerpasan NCEP-CFSR adalah kurang memuaskan, dengan nilai NSE dan R^2 masing-masing 0.87 dan 0.01. Model SWAT yang telah dikalibrasi dengan CMADS digunakan untuk menentukan perubahan dalam jumlah larian air, larian air permukaan, larian air bawah tanah dan evapotranspirasi di MRB di bawah pelbagai senario iklim. Secara umum, jumlah larian air, larian air permukaan dan larian air bawah tanah menunjukkan hubungan positif dengan kerpasan dan hubungan negatif dengan suhu. Sensitiviti jumlah larian air dan larian air permukaan terhadap perubahan kerpasan adalah lebih tinggi pada bulan Mac-Mei dan September-November berbanding Julai-September dan Disember-Februari. Nilai ekstrem tinggi bagi jumlah larian air, larian air permukaan, dan larian air bawah tanah lebih cenderung berlaku antara bulan Mac hingga Mei. Kesan perubahan suhu terhadap jumlah larian air bulanan, larian air permukaan dan larian air bawah permukaan menunjukkan nilai ambang bagi kebanyakan tempoh. Sebaliknya, di bawah kebanyakan senario perubahan iklim, evapotranspirasi menunjukkan hubungan positif dengan kerpasan dan suhu. Secara keseluruhan, evapotranspirasi adalah lebih tinggi di bahagian barat dan tenggara lembangan. Apabila hujan berkurang sebanyak 15% dan 30%, jumlah larian air menurun sebanyak 19% dan 46%. Sebaliknya, apabila kerpasan meningkat sebanyak 15% dan 30%, jumlah larian air meningkat sebanyak 46% dan 81%. Secara ringkasnya, kerpasan mempunyai kesan yang lebih besar terhadap turun naik larian air di MRB berbanding suhu.

SENSITIVITY OF EVAPOTRANSPIRATION AND RUNOFF TO CLIMATE CHANGE IN THE MUDA RIVER BASIN, MALAYSIA

ABSTRACT

Understanding how climate change affects the tropical water balance is crucial for developing innovative strategies to adapt and mitigate climate change. Hydro-climatic evaluation relies heavily on accurate climate data; however, climate research faces challenges in acquiring long-term observed climate data. This study aims to assess the impacts of climate change on water balance in the Muda River Basin (MRB) using open-source data. First, this study evaluates the reliability of the China Meteorological Assimilation Driving Dataset for the Soil and Water Assessment Tool (CMADS) and the National Centres for Environmental Prediction Climate Forecast System Reanalysis (NCEP-CFSR) in simulating climate and hydrological changes in the MRB. The optimal data was then used to run the Soil and Water Assessment Tool (SWAT) model to study the impacts of climate change on the water balance under fourteen synthetic climate scenarios, which include temperature increases by 1.5 °C and 2 °C, along with precipitation changes ranging from -30% to +30%, based on previous literature. The results show that increases in both precipitation and temperature lead to higher runoff. The SWAT model effectively simulates the monthly runoff of the MRB, with NSE and R^2 values of 0.57 and 0.59, respectively. CMADS demonstrated higher accuracy than NCEP-CFSR, with PBIAS and RSR values of 9.2% and 0.66, respectively. The performance of the SWAT model using NCEP-CFSR precipitation data for streamflow simulation was unsatisfactory, with NSE and R^2 values of -0.87 and 0.01, respectively. The calibrated SWAT model, incorporated with

CMADS, was used to determine changes in total runoff, surface runoff, underground runoff, and evapotranspiration in the MRB under different climate scenarios. In general, total runoff, surface runoff, and underground runoff showed a positive correlation with precipitation and a negative correlation with temperature. The sensitivity of total and surface runoff to precipitation changes was higher during March-May and September-November compared to July-September and December-February. Extreme high values of total, surface, and underground runoff were more likely to occur between March and May. The effect of temperature changes on total monthly runoff, surface runoff and underground runoff exhibited a threshold value for most periods. In contrast, under most climate change scenarios, evapotranspiration was positively correlated with both precipitation and temperature. Overall, evapotranspiration is greater in the western and south-eastern regions of the basin. When precipitation decreased by 15% and 30%, total runoff declined by 19% and 46%, respectively. Conversely, when precipitation increased by 15% and 30%, total runoff rose by 46% and 81%, respectively. In summary, precipitation has a larger impact on runoff fluctuation in the MRB compared to temperature.

CHAPTER 1

INTRODUCTION

1.1 Background of Study

Climate change is a well-documented threat to social, economic, and environmental systems (Lee et al., 2015; Meng et al., 2018; Ward et al., 2011). Its impact on water resources, rising sea levels due to global warming, and the reduction of land area pose significant challenges to human survival (Singh, 2012). According to the Fifth Assessment Report of the Intergovernmental Panel on Climate Change (IPCC), the global average surface temperature is projected to exceed 1.5 °C by the end of the 21st century. Climate change directly affects every aspect of the water cycle (Peters-Lidard et al., 2021) and poses serious risks to food security while intensifying desertification and land degradation (Mbow et al., 2017).

Water balance, also known as the water budget, refers to the principle that the total water input in a given system equals the total water output. The law of water balance states that the amount of water entering a system or area is equal to the outflow plus any changes in stored water over time (Sutcliffe, 2004; Viessman et al., 1989). In hydrology, the water balance equation describes the movement of water into and out of various hydrologic systems such as soil columns, watersheds, irrigation areas, or cities. Water budgeting is fundamental aspect of hydrology. According to the United States Geological Survey (USGS), understanding of water budgets and underlying hydrological processes is essential for effective water resource management and environmental planning (Viessman et al., 1989). Observed changes in a region's water budget over time can help assess the impact of climate variability and human activities on water resources. By comparing water budget across different regions, it is possible

to quantify the influence of geology, soil, vegetation, and land use on the hydrological cycle.

Human survival and development depend on the availability of water resources. However, global warming and water shortages of water resources caused by social and economic development impose constraints on regional and national growth. According to the 2020 Global Natural Disaster Assessment Report, floods were the most significant natural disasters affecting the world. Data from the Global Disaster Data Platform indicate that between January 2020 and August 2023, a total of 700 floods occurred worldwide. Similar floods have also impacted tropical countries such as Indonesia and Thailand. In Malaysia, between 1900 and 2022, flood affected 1.181 million people, resulted in 316 deaths, and caused economic losses amounting to USD 3282,514. During 2021-2022 alone, Malaysia experienced 10 major floods, affecting 192,000 people, causing 85 deaths, and resulting in USD 1,460,000 in damages (Global Disaster Data Platform, accessed on August 20, 2023). The impact of climate change on water resources and its adaptation strategies are critical global concerns. Under global warming, water resources systems are becoming increasingly vulnerable, primarily mainly due to more frequent extreme hydrological events, higher uncertainty in water availability, changes in the water cycle process, and shifts in ecological water demand (Neitsch et al., 2011). Climate change significantly affects the water balance, where precipitation is the primary factor influencing runoff. Temperature, in turn, is the key climatic element driving terrestrial evapotranspiration. The extent of climate change impact on the water balance depends on variations in precipitation and temperature, as well as their interact (Arnold et al., 1993).

Freshwater provides a wide range of ecosystem services essential to human well-being. River basins serve as fundamental units for water resource planning and

management. Water balance analysis within river basins is crucial for scientific evaluation and rational allocation of water resources. Time-series data play a vital role in flood disaster prediction, climate change assessment, water quality evaluation, and aquatic ecosystem monitoring (Bourdin et al., 2012; Ravazzani et al., 2015; Smith & Pavelsky, 2008). High-quality river flow forecasting and trend analysis offer multiple benefits, including enhanced water management through improved river inflow predictions, better flood forecasting and monitoring capabilities, and a deeper understanding of river dynamics for future water planning (Le et al., 2019). However, the availability and scarcity of watershed measurement data remain significant challenges in developing countries. The lack of reliable data also hampers the effective water resource management in river basins (Tan, 2016).

Climate data is the most critical components in building a hydrological model. Reliable climate data is essential for improving model accuracy. Traditionally, observations have been the primary source of climate data for hydrological modelling, providing key variables such as precipitation, maximum and minimum temperatures (Zhu et al., 2016). Nevertheless, some satellite and reanalysis products also incorporate observed data for calibration or assimilated to improve their accuracy. Despite this, the lack of observed stations in certain areas, such as remote, high-altitude, and underdeveloped regions, introduces uncertainties and errors in climate data. Radar and satellite precipitation products can help overcome this limitation by providing high-precision observational data. Unfortunately, in some regions, data from measuring stations is not freely accessible due to data-sensitive policies, restricting public access and limiting their use in model calibration. As a result, many observed stations are excluded from the development and calibration of open-source climate data. Consequently, ensuring the reliability of these data for hydrological modelling has

become a critical issue, particularly in developing and less developed countries (Li et al., 2018; Mohammed et al., 2018; Tan et al., 2018; Yang et al., 2014).

The rapid development of satellite technology over several decades has significantly impacted on the field of hydrology, leading to the production of high-quality precipitation datasets and improvements hydrological modelling. While these climate products enhance hydrologic simulations, they may also be affected by uncertainties, unavoidable errors, or other influencing factors (Villarini et al., 2009). For example, the National Centres for Environmental Prediction (NCEP) of the United States provides NCEP-CFSR (Climate Prediction System Reanalysis). However, due to the reanalysis process involved in generating precipitation products, there are inevitable uncertainties in prediction models, input data and data assimilation methods. Therefore, it is essential to evaluate and re-assess the quality of these precipitation products in different regions, and examine their applicability in hydrology and climate studies (Hodges et al., 2011).

The China Meteorological Assimilation Driving Dataset (CMADS) is a newly developed reanalysis grid dataset. It has a spatial resolution of $0.25^{\circ} \times 0.25^{\circ}$ and the open-source covers the time period from 2008 to 2016 (Meng et al., 2018). CMADS data can be applied to various hydrological models, such as the Soil and Water Assessment Tool (SWAT) model, the Variable Infiltration Capacity (VIC) model, and the Stormwater Management Models (SWMM). Additionally, it allows users to easily extract various meteorological variables such as precipitation, temperature, relative humidity, solar radiation, and wind speed for detailed climate analysis. NCEP-CFSR provides standardised reanalysis data, while CMADS offers predicted reanalysis data in comparison to NCEP-CFSR. Studies utilizing CMADS with the SWAT model are primarily concentrated in China, including the applications in the Manas River basin

(Meng et al., 2018), the Fuhe River (Lu et al., 2020), the Qujiang River (Song et al., 2020), and the Jinhua River Basin (Zhou et al., 2019). Overall, CMADS-based simulations using the SWAT model have shown better performance in Chinese river basin. Outside China, a study conducted in the Han River Basin on the Korean Peninsula assessed CMADS data for hydrological simulation, with results indicating moderate performance (Vu et al., 2018). In East Asian countries, including Malaysia, research on CMADS-based river simulations is limited.

NCEP-CFSR and CMADS, as reanalysis datasets, serve as sources and supplements for meteorological data to address the issue of station sparsity (Zhang et al., 2020). NCEP-CFSR is one of the most widely used reanalysis datasets (Saha et al., 2010), while CMADS, as a newer reanalysis dataset, has gained significant attention among scholars and is widely used in China and across East Asia (Cao et al., 2018, 2018; Li et al., 2019; Meng et al., 2019; Meng & Wang, 2017; Vu et al., 2018). Reanalysis data offer advantages such as high quality and improved spatial and temporal resolution (Hodges et al., 2011; Lin et al., 2014). The capability of CMADS was evaluated for the Heihe River Basin, located in the arid region of Northwest China, and it was found that the simulation performance of CMADS combined with the SWAT model was superior to that of CFSR and observations (Meng et al., 2016). However, the quality and reliability of reanalysis datasets can vary across different regions (Hodges et al., 2011; Lin et al., 2014). Therefore, in this study, CMADS and NCEP-CFSR are used to assess their quality and applicability in the study area.

Long-term research has shown that climate change significantly impacts runoff, making it crucial to implement policies that balance economic development and environmental concerns. In the 1970s, the United States National Research Association (USUA) conducted one of the earliest studies on the effects of climate

change on water supply (Douglass et al., 1983). By 1988, climate change had gained global attention, leading the establishment of the IPCC by the World Meteorological Organization (WMO) and the United Nations Environment Programme (UNEP). The IPCC's assessments became the key scientific basis for climate change. In China, Zhu and Zhang (2005) analysed runoff changes in the upper reaches of the Hanjiang River Basin using climate models, finding that higher precipitation or lower temperatures increased runoff. Using the SWAT model, Hu (2015) simulated the eco-hydrological of the Beiluo River in China, revealing challenges regional in the hydrological simulations, with the best accuracy during flood seasons but biases in annual and monthly runoff predictions.

SWAT is currently one of the most widely used hydrological models, with over 4,000 publications (Mannschatz et al., 2016; Tan et al., 2020; Tan, Gassman, et al., 2019). With integrations of geographic information system (GIS) platforms, SWAT is better equipped to represent spatial variations in hydrological changes across complex watersheds. The model offers several advantages: (1) it requires easily accessible input data; (2) it performs well in large-scale watershed simulations; and (3) it has high computational efficiency, allowing for long-term simulations. Therefore, SWAT has been widely applied in areas such as water environment studies, agriculture and forestry ecology in many countries, yielding successful outcomes. Since the model is open-source, users can freely download and modify the source code. With ongoing research, many researchers have optimised its performance. At present, the model is well-developed and mature, with SWAT2009 and SWAT2012 being the most commonly used versions (Boles et al., 2015; Ghobadi et al., 2015; Seo et al., 2014).

The model is mainly used by water scientists to understand the effects of land use and climate change on water quantity and quality (Gassman et al., 2014). For

example, American hydrologist Srinivasan and Arnold (1994) applied the SWAT model to simulate runoff in an Illinois watershed and found that while SWAT was well-suited for long-term simulation. Hanratty and Stefan (1998) used SWAT96 to investigate the impact of climate change on runoff quality and quantity in a northern agricultural watershed in Minnesota. This study emphasized the critical role of model parameter calibration in achieving accurate simulation results. Bingner (1996) applied SWAT to simulate runoff in the Goodwin Creek Watershed in Mississippi with a 10-year period, confirming the model's capability to capture the temporal and spatial changes on runoff. Jimeno-Sáez et al. (2018) compared the SWAT model with an artificial neural network (ANN) model to evaluate runoff estimation accuracy across different climate zones on the Spanish Peninsula. Their findings showed that both models performed well, but SWAT was more effective in simulating low-flow conditions. Thavhana et al. (2018) used QSWAT to calibrate and verify uncertainty parameters in the Luvuvhu River basin in South Africa, facilitating improved basin design and planning. Similarly, Leta et al. (2018) applied the SWAT model to evaluate the hydrological performance of Oahu Island, Hawaii, a tropical island with similarities to Sri Lanka Island. Their study examined runoff simulation effects in both leeward and windward basins, and found that daily runoff simulations were more accurate in the leeward basins. Tan et al. (2019) summarised the application of the SWAT model in Southeast Asia and confirmed its superior performance in model capability assessment, land use assessment, and climate change assessment. However, they also highlighted that more attention is needed regarding the use of SWAT for simulating extreme events. Memarian et al. (2014) used the SWAT model to investigate the effects of land use and cover change (LUCC) on hydrological conditions of the Hulu Langat basin, specifically discharge and sediment load.

The Muda River Basin (MRB) is an important source of freshwater for the northern states of Peninsular Malaysia. Luhaim et al. (2021) used the Standardised Precipitation Index (SPI) and the Standardised Streamflow Index (SSI) to analyse the spatial-temporal changes of historical droughts in the basin from 1985 to 2019. They identified the major drought years, and suggested that future studies should examine whether reduced rainfall or increased temperature plays a more significant role in regional droughts formation. Tan et al. (2021) analysed trends in precipitation and extreme temperature in the basin over the period from 1985 to 2015. In the same study, they also analysed the effects of land use changes on water balance. In fact, assessments of the impact of climate change on water resources remain limited in the MRB (Tan, Yusop, et al., 2017). One possible reason for this is the difficulty in obtaining reliable land use and climate data (Tan, Ibrahim, Yusop, et al., 2015). Therefore, examining meteorological changes holds significant practical importance for the sustainable development and management of water resources (Kundzewicz & Somlyódy, 1997). The integration of CMADS data and future climate scenarios can analyse facilitate the analysis of future runoff changes, thereby enabling more effective formulation of water resources management strategies by the government.

1.2 Problem Statement

Accurate climatic data are essential for improving model accuracy. Inaccurate climate data can lead to ineffective water resource management. Surface stations collect precipitation data, but quantifying it remains challenging. Due to their uneven distribution, these stations rarely provide high-precision data (Miao et al., 2015; Steiner et al., 2003). Global reanalysis data are widely used to supplement the deficiencies of ground-measured precipitation data, as they offer high spatial and

temporal resolution (Bao & Zhang, 2013; Chen et al., 2014; Fuka et al., 2014; Largeron et al., 2015; Ward et al., 2011). CMADS data are considered reliable and are widely utilized in East Asia and other countries. However, they have been minimally explored in tropical regions such as the MRB in Malaysia, and their accuracy remains uncertain. CMADS data are significant for research due to their open-source accessibility, high accuracy, fine resolution, and compatibility with various formats. Researchers can easily use CMADS data to drive hydrological models and enhance climate assessments.

Global climate change affects the hydrological cycle, with runoff and evapotranspiration being closely linked to the spatial and temporal distribution of water resources. However, there are numerous uncertainties and debates regarding the response and sensitivity of runoff and evapotranspiration to climate change, and comprehensive region-specific assessments remain limited. Research on the MRB has primarily focused on land use changes, precipitation patterns, and drought trends, with little emphasis on the impact of climate change on runoff and evapotranspiration. These hydrological processes are highly complex and spatially heterogeneous due to the wide variations in physical geography and climate across different regions.

Climate change poses a significant threat to hydrological systems and global water resources. Evapotranspiration and runoff are influenced by climatic factors such as temperature, precipitation, humidity, wind speed, and solar radiation (Allen et al., 1998; Trenberth et al., 2003). For example, rising temperatures can intensify precipitation but also increase evaporation and the frequency of dry spells. Shifts in temperature and precipitation patterns alter evapotranspiration rates, exacerbating water shortages (Fisher et al., 2011). Additionally, greater precipitation amplitude, e.g., heavy rainfall events, leads to higher surface runoff, increasing flood risks. Runoff, which flows across land into waterways, depends on precipitation intensity, soil

moisture, and land cover (Milly et al., 2005). Climate change can intensify these factors, leading to more frequent and severe floods and droughts, impacting both ecosystems and human populations (IPCC, 2023). However, in-depth analyses of their sensitivity is relatively limited in the literature, which is important for predicting water resource changes, formulating effective water resource management strategies, and mitigating the effects of climate change.

1.3 Research Questions

In this study, the research questions are as follows:

RQ1: Which long-term gridded precipitation products is suitable for estimating precipitation over the MRB?

RQ2: How do evapotranspiration and runoff respond to temperature or precipitation changes, respectively, in the MRB?

RQ3: How sensitive are evapotranspiration and runoff to the combined effects of temperature and precipitation changes in the MRB?

1.4 Research Objectives

In this study, the research objectives are as follows:

RO1: To evaluate the reliability of CMADS and NCEP-CFSR for estimating precipitation over the MRB.

RO2: To analyse the individual responses of evapotranspiration and runoff to changes in temperature and precipitation in the MRB.

RO3: To assess the sensitivity of evapotranspiration and runoff to the combined effects of temperature and precipitation changes in the MRB.

1.5 Significance of the Study

Currently, droughts and floods have caused significant economic losses. In recent decades, climate change has led to an increase in the frequency and intensity of rainfall events (IPCC, 2023). As a result, water runoff has increased, leading to greater fluctuations in water flow. Malaysia faces serious challenges during the monsoon season, including floods, soil erosion, and other natural disasters. Flooding not only submerges vegetation and damages infrastructure but is also accompanied by severe soil erosion. Over the past 20 years, Malaysia's urbanization has expanded by 40%, leading to increased surface runoff and reduced natural infiltration (Department of Statistics Malaysia, 2022). Studies indicate that certain soil types, such as clayey soils, are particularly vulnerable to erosion under heavy rainfall (Smith et al., 2011). Over the past decade, agricultural lands in Malaysia have experienced a 15% increase in erosion.

As development increases, so does the demand more for materials required by human beings, which in turn expands land development and raises the demand for minerals. This leads to issues such as soil erosion, landslides, mudslides, earthquakes, and other ecological problems. Understanding the influence of climate change on runoff processes is of great importance. This helps to reduce the damage caused by soil erosion and alleviate non-point source pollution and other environmental issues in the MRB. The research findings are valuable for the Malaysian government in formulating water resources management plans. The findings of this research also serve as references for the IPCC Working Group. Furthermore, the assessment of reanalysis climate data provide alternative data source for supporting hydro-climatic and disaster research, enhancing data availability. It also increases the confidence of

researchers who cannot access observed precipitation data and offers guidance on selecting suitable open-source precipitation products.

Finally, based on the Paris Agreement and existing literature, different climate scenarios were established to analyse how global initiatives could affect hydrological responses under global warming scenarios of 1.5 °C and 2°C. The most important climate factors affecting runoff changes were explored to provide data support for water resource planning and management in the basin, lay the foundation for the formulation of local water resource management policies, and offer recommendations for government and researchers.

1.6 Scope of the Study

The first part of the study involves building a SWAT-based model for the MRB. The input data sets include DEM, climate data, observed streamflow data, soil map, and land use map. The DEM was generated from satellite data, while the observed climate, streamflow, and soil map were collected from related government agencies or open-source websites.

The Sequential Uncertainty Fitting-2 (SUFI-2) parameter verification algorithm, under SWAT Calibration and Uncertainty Procedures 2012 (SWATCUP 2012) software, was used for the calibration. The advantage of this algorithm is that it combines model structure and uncertainty analysis of the input data. After 1000 repeated iterations, the model autonomously finds the optimal values, and the sensitivity results of the parameters are obtained. The T-test is used to assess parameter sensitivity, and both the *p*-value and T-value are considered. CMADS and NCEP-CFSR were selected for the assessment because they are widely applied in different parts of the world. The established climatic scenarios were used as inputs in the

calibrated SWAT model to evaluate the effects of climate change on runoff and evapotranspiration in the MRB.

1.7 Structure of Thesis

This thesis consists of five chapters. The first chapter introduces the research background, problem statement, research objectives, research scope, and thesis structure.

The second chapter covers the topics of the hydrological cycle, hydrological modelling, remote sensing in hydrological modelling, CMADS and NCEP-CFSR data uncertainty assessment, land use change, and climate change scenarios, and studies related to climate change runoff in Malaysia.

The third chapter introduces the research method, the general characteristics of the selected research area, the description of the SWAT basic data set, an introduction of precipitation products, the principles of the SWAT model, modifications and establishment of the SWAT model, parameter calibration and validation, the setting of climate hypotheses, and the analysis of the impact of climate change on runoff.

The fourth chapter presents the result analysis. The selection of sensitive parameters, calibration, and verification of the SWAT model was done with observed streamflow in MRB. In addition, a comparison of the precipitation and runoff trends under the selected two precipitation products is provided. The simulation effects of CMADS data and NCEP-CFSR data in MRB were evaluated separately. On the other hand, changes in total runoff, evapotranspiration under different precipitation and temperature scenarios are analysed, along with their combined impacts based on year, season, and month.

The fifth chapter summarized the reliability of different precipitation products in the MRB, and the hydrological response results under different climate scenarios. Lastly, suggestions for future research are provided.

CHAPTER 2

LITERATURE REVIEW

2.1 Introduction

Climate has a profound effect on the Earth's environment. The Earth's climate is shaped by the interaction of the five components: the atmosphere (air), the hydrosphere (water), the cryosphere (ice and permafrost), the lithosphere (the Earth's upper rock layer), and the biosphere (living organisms). According to the WMO, climate is defined as the average of meteorological variables such as temperature, precipitation and wind over 30-year periods (Parry, 2007).

Climate change refers to long-term changes in the state of the climate. It is typically reflected in statistical differences in meteorological variables, such as temperature and precipitation, over different time periods. Climate change is considered a statistically significant alteration in the mean state of the climate or a change that lasts for an extended period, typically 30 years or more. It includes not only changes in mean values but also changes in variability. The term climate change, as used by the IPCC, refers to any change in climate over time, whether due to natural variability or human activity.

The Working Group I report of the Sixth Assessment Report of the United Nations-led IPCC concluded that, under all emissions scenarios, global warming will reach at least 1.5 °C. In the low-emission scenario, global warming is projected to reach 1.5 °C in the 2030s, slightly exceed the temperature control target with a peak of 1.6 °C and then decline to 1.4 °C by the end of the century. This temperature increase may lead to the occurrence of floods in arid river regions across the globe.

Any change in climate can impact on both natural ecosystems and socio-economic systems. Studying the environmental and economic causes of climate change, as well as

addressing its potential impacts, is vital for policymakers in planning the future direction of a country. To support this, the IPCC was established in 1988 by the WMO and the UNEP serves as an international organisation that provides the best available scientific information on the global social and economic impacts of climate change and offers assessment and countermeasures.

Water is a renewable resource that humans can use repeatedly (Oki & Kanae, 2006). Despite Earth is known as the “blue planet”, water-related problems persist. Global freshwater scarcity and the insecurity caused by contaminated drinking water remain pressing issues. Only 2.5% of the Earth's water is freshwater, most of which exists as glaciers or deep groundwater (Khilchevskiy & Karamushka, 2020).

After extensive research, the international scientific community has reached a consensus on the significant impact of climate change on global and regional hydrological processes. These changes, along with the increased intensity and frequency of extreme hydrological events, pose important challenges for future water resource management. Therefore, many scholars have assessed and investigated the effects of climate change on runoff (Fowler et al., 2007; Govender et al., 2022; Kundzewicz & Somlyódy, 1997; Prudhomme et al., 2002; Shu et al., 2018; Sonali & Nagesh Kumar, 2020; Stein et al., 2021).

2.2 Hydrological Cycle

The interaction between the water cycle, atmosphere, rocks, glaciers, and biospheres constitutes the fundamental physical processes of the Earth system (Lovelock, 2016; Schneider, 2004). The hydrological cycle refers to the continuous movement of water in the forms of liquid, solid, and gas in the climate system. It can be stored in the oceans, ice sheets, land surface, and atmosphere. It is one of the most dynamic and crucial components in the interactions between the ocean, land, and atmosphere (Oki & Kanae, 2006; Trenberth et al., 2003).

As the ambient pressure steadily decreases during the rising water vapour process, suspended water droplets or ice crystals in the atmosphere gradually transform, forming clouds. As temperature drops and volume increases, larger clouds can overcome air resistance and produce precipitation without dissipating. The continuous condensation of water vapor molecules on cloud surfaces, along with the merging of clouds of different shapes, causes them to expand. Eventually, the clouds grow large enough to generate precipitation in the form of rainfall, snowflakes, or other types, which then fall to the ground. Some of this precipitation evaporates upon contact with vegetation and other surfaces, returning to the atmosphere.

Soil moisture, which infiltrates the ground through various pathways, supplements precipitation that seeps into the soil. Water eventually returns to the atmosphere after evaporation from soil surfaces (Seneviratne et al., 2010). Soil moisture plays a crucial role in enhancing the land's water retention capacity and serves as an essential reservoir for Earth's water resources. Groundwater enters the subsurface through two main pathways: (1) infiltration through soil, and (2) percolation through rock pores. Groundwater, which exists within soil and rock pores, often flows over considerable distances before emerging at the surface. Overall, water storage occurs in two primary state including evaporation and infiltration into the ground. As surface water flows, some of it evaporates while some infiltrates into the ground. The remaining water continues to flow into the ocean through streams and rivers, completing the water cycle.

The hydrological cycle, essential for maintaining ecosystem balance, involves the complex and systematic processes of evaporation, condensation, precipitation, infiltration, and runoff. Evaporation, primarily occurring on the surfaces of oceans, lakes, rivers, and soils, is driven by solar energy, converting water from liquid to vapor and significantly influencing atmospheric moisture levels. As water vapor rises, it condenses to form clouds, which return to the surface as precipitation when sufficient moisture accumulates.

Upon reaching the ground, some precipitation infiltrates the soil, while excess water surpassing the soil's infiltration capacity generates surface runoff, which flows into rivers, lakes, and oceans. The formation and magnitude of runoff are influenced by precipitation intensity, land slope, soil saturation, and land use. The hydrological cycle plays a crucial role in distributing heat and water on a global scale, helping regulate Earth's climate. Evaporation absorbs heat, while condensation releases it, balancing temperature and humidity levels.

Over the past century, the distribution, intensity, and extremes of global precipitation, evapotranspiration, water vapor, and runoff have shifted in response to rising temperatures, indicating that global warming is intensifying the hydrological cycle (Kramer et al., 2015). However, due to significant regional variations and limitations in the spatial and temporal coverage of monitoring networks, considerable uncertainty remains regarding trends in hydrological cycle variables (Huntington et al., 2018; Kramer et al., 2015).

2.2.1 Tropical Hydrological Cycle

Hydrological cycle processes are accelerating in the tropics due to rising temperatures and increased air humidity. The tropics, located near the equator, experience high temperatures and heavy rainfall throughout the year. However, precipitation is unevenly distributed and shows high inter-annual variability, largely influenced by monsoonal patterns. The humid tropics, specifically situated between latitudes 25°S and 25°N, experience an average of 270 days per year where precipitation exceeds evaporation (Wohl et al., 2012). The tropical hydrological cycle is shown in Figure 2.1.

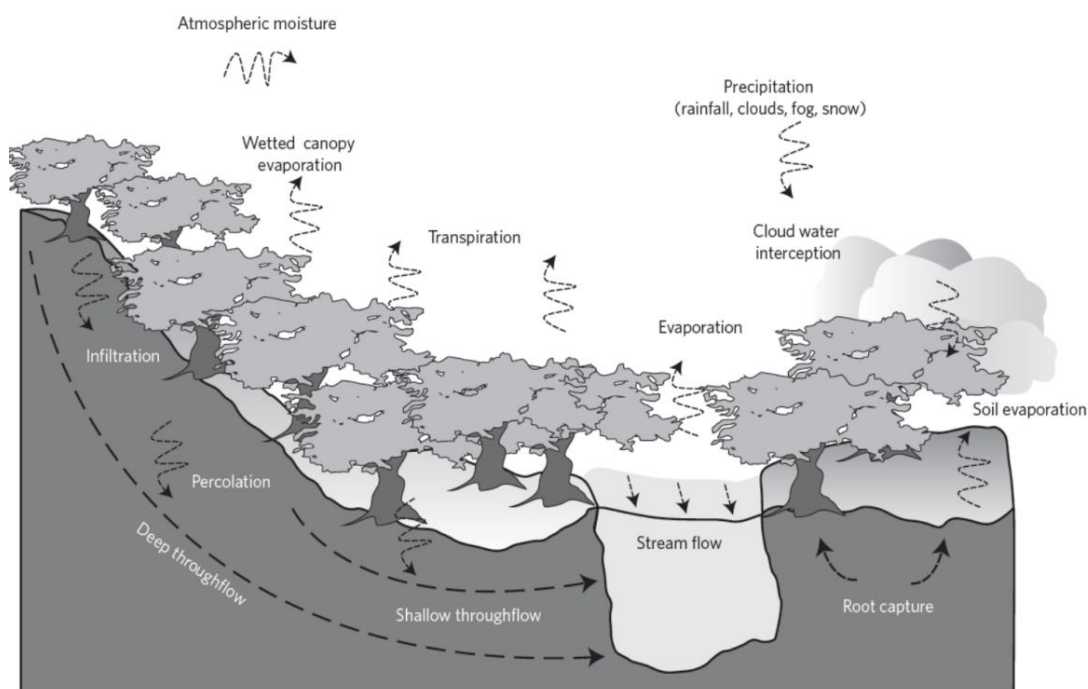


Figure 2.1 Tropical hydrological cycle (Wohl et al., 2012).

Temperature and air moisture levels in tropical regions differ from those in mid-latitude zones. Additionally, the impact on river elements such as suspended sediments and streamflow is more pronounced due to the higher intensity and greater inter-annual variability of precipitation in the tropics (Wu et al., 2006).

2.2.2 Runoff

Precipitation in the basin flows into the river network through both surface and sub-surface, and the water that exits the outlet of the basin is called runoff (Chow, 1965; Dunne & Leopold, 1978; Ward & Robinson, 1967). Understanding the key factors influencing runoff components, as well as the contributions of precipitation and temperature, is crucial for water-limited inland basins (Wang et al., 2023). Runoff plays a vital role in the Earth's water cycle. It is the flow of water generated by atmospheric precipitation that enters rivers, lakes, or oceans through various pathways within the basin. Runoff also commonly refers to the volume of water passing through a specific river section over a given period. The frequent occurrence of extreme precipitation poses a serious threat to both the socio-economic systems and natural ecosystems.

Therefore, studying the impact of climate change on runoff is of practical significance (Zhou et al., 2024).

Human activities such as tillage, reclamation, and land use changes affect runoff by reducing soil moisture, leading to soil erosion, flood disasters, and other environmental issues (Pimentel et al., 1995). The construction of water storage structures such as reservoirs, enhances the basin's capacity of store water and helps regulate runoff. As a key component of the surface water cycle, runoff significantly influences hydrological processes (Dingman, 2015).

In general, runoff characteristics refer to quantitative measurements such as the annual average discharge, monthly average discharge, maximum annual flood discharge, and minimum low-flow discharge. This specific flow information plays an important role in water resource management and engineering design.

2.3 Climate Change Impact on Hydrology

Although the study of climate change began earlier, but its impact on water resources only started to attract academic attention in the 1980s. In 1985, the WMO published the first comprehensive assessment report on the impact of climate change on water resources, which summarised the test and sensitivity analysis methods for impact assessment. In 1987, the International Association of Hydrological Sciences organised a symposium themed “Climate Change and its Impact on Hydrology and Water Resources”. Since the 1990s, research on this topic has developed rapidly.

Numerous studies have been conducted to assess the impact of historical climate change on hydrological cycle processes and water resources in various watersheds. Immerzeel et al. (2010) systematically analysed the sensitivity of upstream water resources to climate change in five major watersheds in Southeast Asia. Their findings revealed that the Indus and

Brahmaputra River basins are particularly sensitive to climate change due to their high snowmelt runoff ratio, dense populations, and high irrigation water demand.

Analyses of historical climate data and water resources in the Yangtze and Yellow River Basins in China show that since the 1990s, both temperature and precipitation have increased significantly. As a result, water resources in the Yangtze River Basin have also increased, likely due to accelerated glaciers melting caused by global warming. In contrast, the Yellow River Basin shows no significant trend in water volume, as the effects of increased precipitation are largely offset by increased evaporation, resulting in some fluctuations but no substantial long-term change (Wang et al., 2013).

Northwest China experienced significant climate change during the second half of the 20th century (Chen et al., 2015). Sensitivity analyses of water resources to climate change show that, especially in the Xinjiang Autonomous Region, both precipitation and water availability have increased significantly since the 1980s. However, the region has also seen a rise in drought risk. The impact of precipitation varies across regions, with some regions being more sensitive than others. For example, the Hexi Corridor and parts of Inner Mongolia exhibit the highest sensitivity of water resources to climate change (Wan et al., 2015). Xu et al. (2014) quantitatively analysed the water-energy coupling equation in the Haihe River basin to examine the effects of climate and land use changes on runoff. Their findings indicate that the reduction in water resources was primarily due to decreased precipitation, with precipitation change accounting for 26.9% of the variability in watershed runoff. Therefore, in climate change scenario modelling, incorporating precipitation changes as a key factor is both important and feasible when studying runoff variations.

Climate change significantly impacts the water balance, Precipitation is the primary factor affecting runoff, while temperature mainly influences land surface evapotranspiration. Both precipitation and temperature can alter the water balance, with the degree of impact

depending on the magnitude of changes in these two factors and their relationship. The climate scenario setting is also based on the combined effects of temperature and precipitation (Arnold et al., 1993).

However, most research focuses on the response of water resources to future climate change scenarios. Given the uncertainty surrounding future climate change, it is often necessary to use indirect methods to incorporate these scenarios into basin hydrological models and assess changes in basin hydrology and water resources under hypothetical conditions. This approach is referred to the “what-if-then” approach by IPCC.

2.4 Evapotranspiration, Runoff and Sensitivity Analysis

Evapotranspiration is a crucial component of the hydrological cycle and a key factor influencing water resource availability. While changes in precipitation directly impact river runoff, global warming and rising temperatures affect potential evapotranspiration, which in turn indirectly influences surface runoff. Therefore, conducting sensitivity analyses of evapotranspiration and runoff in response to climate change is essential.

The Sixth Assessment Report of the IPCC states that, depending on different greenhouse gas emission scenarios, global temperatures could rise by 1.5 to 5.7 °C by the end of the 21st century (IPCC, 2023a). The report highlights that precipitation is expected to increase significantly at high latitudes and near the equator, while it is likely to decline in arid mid-latitude and subtropical regions. Additionally, the frequency and intensity of extreme weather events, such as heavy rainfall and droughts, are projected to rise, posing significant challenges for global water resource management.

In recent years, researchers worldwide have extensively studied river runoff attribution and the impacts of climate change. Developing watershed hydrological models tailored to specific study areas is crucial for accurate assessments (Fan et al., 2021; Wang et al., 2022).

Analyses based on uncertainty theory indicate that climate scenarios and evaluation models are the primary sources of uncertainty in assessment results. Among these, climate scenario uncertainty has a significantly greater influence than the evaluation model or other factors (Hao et al., 2007). To assess the sensitivity of water resource systems to climate change, scenario-based analyses reflecting climate trends are employed for water resource planning and development. The IPCC defines sensitivity as the degree to which a system is affected by climate-related stimuli, encompassing both positive and negative impacts (IPCC, 2023a). Climate-related stimuli include the average climate state, climate variability, and the frequency and intensity of extreme events, with both direct and indirect consequences. In water system sensitivity studies, climate change scenarios typically incorporate variations in precipitation and temperature. A stronger response under the same scenario indicates higher sensitivity of the hydrological element, and vice versa. Sensitivity analyses, therefore, provide crucial insights into the potential impacts of climate change on water resources.

2.5 Climate Change Impacts on Water Resources

There are two approaches to studying the impact of climate change on water resources. The first is the application of more extensive statistical analysis, which requires a large amount of hydro-meteorological and other observation data. The second approach is hydrological modelling, which is a well-conceived and effective tool for assessing water resources and eco-hydrological impacts. However, there are some uncertainties in hydrological modelling methods, and an important issue remains in linking meteorological data to hydrological models. In the Haihe River Basin, Wang et al. (2008) simulated the response of water resource changes to climate change and concluded that the water resources in the basin showed a situation of reduction and shortage. The increase in temperature and evaporation caused by climate change increased the proportion of water reduction by 2% to 4%. Githui et al. (2009) used the SWAT

model to simulate and analyse the Nzoia basin. They found that rainfall has a greater impact on the change in runoff as compared to temperature.

With the development of research, the IPCC introduced Representative Concentration Pathway (RCP) scenarios in the fifth assessment report, which has been widely used and recognised by countries around the world. The RCP scenarios are conducive to predicting future climate change and has high accuracy in predicting future climate change trends (Zhan et al., 2013). The impact of future climate scenarios on river basin runoff will continue to deepen.

2.6 Hydrological Modelling

The hydrological model is one of the fundamental methods to simulate hydrological processes in hydrological science. It relies on mathematical principles, meteorological and hydrological data, and practical human beings. Hydrological models, also known as runoff models or watershed models, first appeared in the late 19th century. The development of these models has played an important role in advancing the application of hydrology and the effective management of water resources (Bourdin et al., 2012; Todini, 1988).

The primary research and application focus of the hydrological model is on runoff, and climate data serves as a key factor driving the model and influencing runoff simulation. The hydrological model is an essential tool to simulate the hydrological process and understand the hydrological behaviour of the basin. It has significant practical importance for the calculation of runoff generation, flood analysis, optimal allocation and scheduling of water resources, and assessing the impacts of climate and land use change. The hydrological model also supports governments in formulating more effective water resources management policies.

Hydrological models can typically be classified based on spatial distribution, model process complexity and time scale, whether long-term or short-time. Several classification methods are shown in the Figure 2.2 (Bourdin et al., 2012; Singh & Woolhiser, 2002). The